

Effective sine-Gordon model for the static properties of narrow window junctions

Jean-Guy Caputo

*Laboratoire de Mathématiques, INSA, and U.P.R.E.S.A. C.N.R.S. 60-85, BP8,
76131 Mont-Saint-Aignan Cedex, France*

Nikos Flytzanis,^{a)} Vladislav Kurin,^{b)} and Nikos Lazarides

Department of Physics, University of Crete, 71409 Heraklion, Greece

Emmanuel Vavalis

*Mathematics Department, University of Crete, 71409 Heraklion, Greece and IACM, FORTH,
71110 Heraklion, Greece*

(Received 20 March 1998; accepted for publication 13 August 1998)

We show that the maximum tunneling current for a long thin window Josephson junction in the presence of an external magnetic field is given to a good approximation by the solution of an effective sine-Gordon model with appropriate rescalings. This model is obtained via a reduction of the two-dimensional system to a one-dimensional integro-differential equation (nonlocal sine-Gordon). The passive region introduces an effective Josephson characteristic length. Using numerical simulations we show that for a narrow junction the cases of inline and overlap current feed are well described by the effective model. We discuss the influence of the width of the junction and find that the model gives a good approximation for the behavior of large area windows in the inline geometry, while it deviates for the overlap. © 1999 American Institute of Physics. [S0021-8979(99)02122-7]

I. INTRODUCTION

A Josephson junction is a weak link between two superconducting films across a thin oxide layer allowing the tunneling of Cooper pairs and/or quasiparticles.^{1,2} Its electromagnetic properties as an oscillator can be described by a sine-Gordon equation for the phase difference of the macroscopic order parameters in each film. This model has been successfully used to describe a variety of static and dynamic effects for long junctions whose length is much larger than the Josephson penetration length λ_J .³ In practice, however, the technology of fabrication of modern Josephson junctions, which stems from the technology of semiconductors, is such that the top and bottom superconducting plates occupy an area larger than the one of the junction itself and forms an “overhang” leading to a so-called “passive region” due to the large thickness of the intermediate insulating layer around the junction. This serves as protection of the interface from mechanical damage as well as a cavity to which the oscillator can couple with adjustable impedance mismatch, thus increasing the output power of the device.

The passive region contributes significantly to the static and dynamic properties of these window junctions. A systematic variation of the extension w' of the passive region for a long junction has shown in particular that its presence can lead to the disappearance of the “zero-field step” dynamical states corresponding to the shuttling of a soliton inside the window.⁴ The static behavior of these devices,

which is characterized by the maximum current flowing through the junction for a given magnetic field and provides an important way to calibrate them, is also strongly affected. The maximum current for zero magnetic field increases with w' and the critical magnetic field H_c corresponding to the vanishing of the current decreases.⁴ Another experimental study by the group of Salerno⁵ emphasized the different roles played by a lateral or longitudinal passive region for long junctions. It showed that a lateral passive region causes an increase of the velocity of the linear waves in accordance with the result on the dispersion curve obtained by Lee,⁶ while a longitudinal passive region only acts as a lumped capacitance on both ends of the junction.

We have emphasized the fundamental role of the lateral passive region for window junctions by considering static fluxon solutions.⁷ We showed that the fluxon width in such a system is not given by λ_J as in the case of a pure junction, described by the sine-Gordon equation, but by a larger characteristic length of magnetic flux variation λ_{eff} which in the case of a large passive region causes the inflation of the fluxon and its destruction for a finite length junction. In Ref. 7 we gave limiting expressions for λ_{eff} and showed that λ_{eff} can be used for a quantitative understanding of the behavior of the maximum current I_{max} for a given magnetic field H . Here we confirm and extend this approach by showing that the $I_{\text{max}}(H)$ curve for both inline and overlap geometries can be accurately described by an effective one dimensional model and appropriate rescalings with λ_{eff} . This approach is justified in the case of a narrow junction by a reduction of the two-dimensional (2D) partial differential equation (PDE) system describing the problem to a 1D integro-differential

^{a)}Electronic mail: flytzani@physics.uoh.gr

^{b)}Also at: Institute for Physics of Microstructures, RAS, Nijny-Novgorod, Russia.

equation of the sine-Gordon type where the passive region contributes to the integral term in the form of mutual inductance. This method relies on the resolution of the Laplace problem in the passive region and its subsequent coupling to the equation in the junction, and it is common in the theory of antennas⁸ or for treating surface waves in hydrodynamics.⁹ The nonlocal term can be shown to give a rescaling of the second space derivative and justifies the effective 1D sine-Gordon approach. At this point it is worth noting that an effective model and rescaling was intuitively suggested in Ref. 10 to fit some $I_{\max}(H)$ curves for the overlap geometry. Here we prove the validity of this approach in both inline and overlap geometries and confirm it by comparison to the 2D numerical solution.

In Sec. II we will study the case of an infinitely long and thin window and obtain the integro-differential equation describing the phase in the window and recover the expressions for λ_{eff} obtained by a Rayleigh–Ritz variational procedure in Ref. 7 in the extreme limits of small and infinite idle region. In Sec. III we consider the case of a finite length thin junction. Similarly an integro-differential equation can be obtained, which leads to the effective model. In Sec. IV we compare the results for $I_{\max}(H)$ calculated from the numerical solution of the 2D PDE problem with the effective model in the inline and overlap geometries. In Sec. V we discuss the limitations of this approach, in particular for large area junctions, and include our conclusions.

II. MODEL FOR AN INFINITELY LONG WINDOW JUNCTION

Using as units of spatial dimension the Josephson length λ_J (defined in terms of parameters of the pure junction), the normalized phase difference between the two superconductors forming a window junction is given in the static case by the following system of coupled PDEs⁷

$$\Delta\phi = \sin\phi \text{ in } S_j, \tag{1}$$

$$\Delta\psi = 0 \text{ in } S_p, \tag{2}$$

where ϕ and ψ are the normalized phase differences in the junction (domain S_j) and passive region (domain S_p), respectively [see Fig. 1(a)], and $\Delta \equiv \nabla^2$ is the Laplacian operator. In the following we use three different geometries: (a) a perimetric passive region of width w' all around the window and finite window dimensions $\ell \times w$ [see Fig. 1(a)]; (b) an infinite lateral window [see Fig. 1(b)] with w (w') the width of the window (passive) region; (c) a finite length ℓ lateral window [Fig. 1(c)]. In this section we consider the geometry of Fig. 1(b).

The equations are coupled by the following continuity conditions for the phase and surface current on the junction-passive region interface S_i :

$$\phi = \psi \text{ and } \frac{\partial\psi}{\partial n} = L_{PJ} \frac{\partial\phi}{\partial n}, \text{ on } S_i \tag{3}$$

and the boundary conditions on the external boundary of the passive region S_o

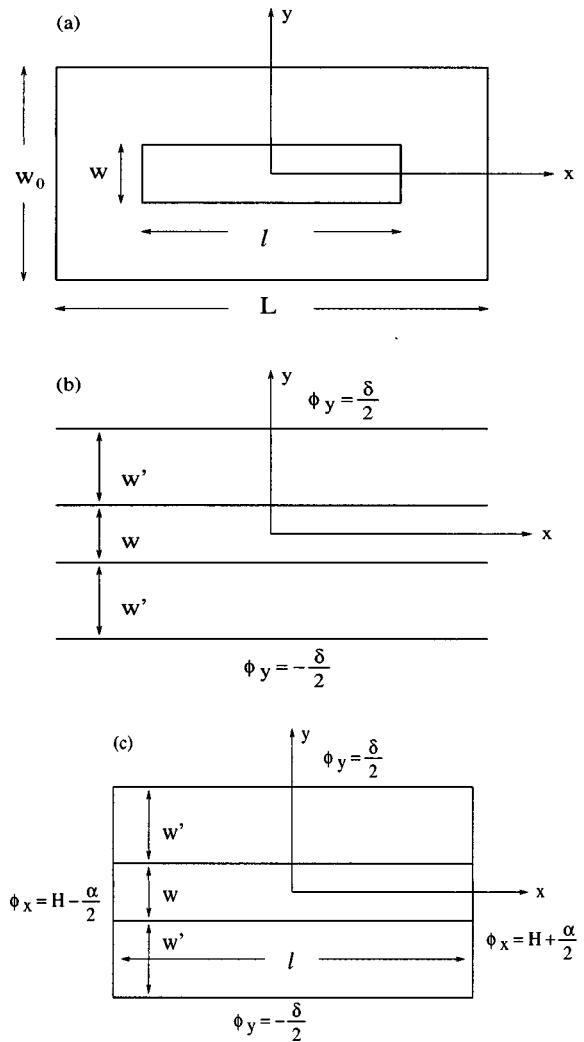


FIG. 1. Schematic drawing of (a) a window junction with mixed passive regions; (b) an infinitely long lateral window junction; (c) truncation of the device shown in (a) eliminating the longitudinal passive region.

$$\frac{\partial\psi}{\partial n} = L_{PJ} I_{\text{ext}}, \text{ on } S_o, \tag{4}$$

where $\partial/\partial n$ denotes the outward normal derivative and I_{ext} is due to an external bias current or applied magnetic field and has been normalized by $\phi_0/L_J\lambda_J$, where ϕ_0 is the flux quantum. The quantity $L_{PJ} = L_P/L_J$ is the ratio of the surface inductances (with L_J to be used as inductance unit) assumed for simplicity constant in the passive region and junction area. In the following we will assume $L_{PJ} \equiv 1$, which describes a small thickness insulating layer in the passive region ($t \ll \lambda_L$, but larger than the oxide thickness t_0) so that the critical current vanishes in the passive region but the inductance is unaffected.

For an infinitely long window junction [Fig. 1(b)] in the x direction, the passive region (S_p) corresponds to $w/2 \leq |y| \leq w/2 + w'$ and the window (S_j) to $|y| \leq w/2$, with interface (S_i) the lines $y = \pm w/2$. The boundary conditions in Eqs. (3) and (4) now become

$$\begin{aligned} \phi|_{y=\pm w/2} &= \psi|_{y=\pm w/2}, & \phi_y|_{y=\pm w/2} &= \psi_y|_{y=\pm w/2}, \\ \psi_y|_{y=\pm(w/2+w')} &= \pm \delta/2, \end{aligned} \tag{5}$$

in the case of an overlap current feed of density δ . In the earlier equations the subscripts represent derivation with respect to the variable.

The solution of the lateral window narrow junction involves four steps, not necessarily in the order presented:

- (i) Solve the Laplace equation in the passive region. This is possible if we assume that the inwards current flow normal to the interface with the window is given by an unknown yet function $I(x)$ [$I(x)/2$ at each interface]. Since the outside boundary conditions are known the solution for $\psi(x,y)$ is given in terms of $I(x)$, which must be determined self consistently by matching the solution and its normal derivative on the interface of the two domains.
- (ii) Assume that the window is narrow and integrate the 2D sine-Gordon equation over the thickness of the window. This requires the introduction of an averaged x -dependent phase $\Phi(x)$ in the window, while the 2D sine-Gordon equation with boundary conditions turns into a 1D equation driven by the interface current $I(x)$.
- (iii) Match ψ and Φ on the interface to express the unknown $I(x)$ in terms of the averaged phase $\Phi(x)$.
- (iv) Solve the resulting nonlocal sine-Gordon equation.

The technical details and the reasoning behind the earlier steps follow. We start by averaging of $\phi(x,y)$ across y in the narrow window,

$$\Phi(x) = \frac{1}{w} \int_{-w/2}^{w/2} \phi(x,y) dy. \tag{6}$$

Assuming $w \ll 1$ so that the average of $\sin \phi$ is close to $\sin \Phi$,¹¹ we obtain from Eq. (1)

$$-\Phi_{xx} + \sin \Phi = \frac{1}{w} [\phi_y]_{-w/2}^{w/2} \equiv I(x), \tag{7}$$

where $I(x)$ is a function to be determined. It corresponds to the surface current normal to the junction-passive region interface and acts as a spatially distributed overlap-like driving current. In Eq. (7) we assumed even y symmetry for ϕ , i.e., $\phi_y|_{y=\pm w/2} = \pm w(I/2)$. We should also remark that in the averaging of Eq. (6) it is not necessary to assume small w . What is important is that the variation of $\phi(x,y)$ with y is small. In fact due to the nonlinearity there will be little variation for w up to the characteristic length (in this case λ_{eff} instead of λ_j). This is the reason why the 1D sine-Gordon model seems to work well in the pure junction.

In the passive region using the y symmetry we need only to consider the Laplace problem in the upper half ($w/2 \leq y \leq w/2 + w'$) with the following Neumann boundary conditions on S_i and S_o correspondingly:

$$\psi_y|_{y=w/2} = w(I/2) \quad \text{and} \quad \psi_y|_{y=w/2+w'} = \delta/2, \tag{8}$$

by using a Fourier transform in x . Notice however that the Fourier transform of ψ in general does not exist because the function does not decay at infinity. We therefore apply the Fourier transform to its first derivative ψ_x

$$\psi_x(x,y) = \frac{1}{2\pi} \int_{-\infty}^{+\infty} dk e^{ikx} \tilde{\psi}_x(k,y),$$

where $\tilde{\psi}_x(k,y)$ is the Fourier transform of $\psi_x(x,y)$. This way we obtain the equation

$$-k^2 \tilde{\psi}_x + \tilde{\psi}_{xyy} = 0,$$

whose solution is

$$\begin{aligned} \tilde{\psi}_x(k,y) = ikA \cosh[k(y-w/2)] \\ + ikB \sinh[k(y-w/2)], \quad y > 0, \end{aligned}$$

and where the coefficients A and B are obtained from the boundary conditions (8)

$$A = \frac{\tilde{\delta} - w\tilde{I} \cosh kw'}{2k \sinh kw'} \quad \text{and} \quad B = \frac{w\tilde{I}}{2k}. \tag{9}$$

\tilde{I} and $\tilde{\delta}$ are the Fourier transforms of I and δ . From Eq. (9) we can solve for $\tilde{I}(k)$, while $A(k)$ can be eliminated in favor of $\tilde{\Phi}(k)$, since the matching at the interface gives

$$\tilde{\Phi}_x(k) = \tilde{\psi}_x(k, w/2) = A, \tag{10}$$

by identifying $\psi(x, w/2)$ with $\Phi(x)$ for small w . Thus $I(x)$ can be eliminated from Eq. (7) if we extract $\tilde{I}(k)$ from Eqs. (10) and (9) and apply the inverse Fourier transform to obtain

$$I(x) = \frac{1}{w} \frac{1}{2\pi} \int_{-\infty}^{+\infty} dk e^{ikx} \left[\frac{\tilde{\delta}}{\cosh kw'} + 2i \tanh(kw') \tilde{\Phi}_x \right], \tag{11}$$

which can be replaced in Eq. (7) to yield the final integro-differential equation describing the thin window junction

$$\begin{aligned} -\Phi_{xx} + \sin \Phi = \frac{1}{w} \frac{1}{2\pi} \int_{-\infty}^{+\infty} dk e^{ikx} \frac{\tilde{\delta}(k)}{\cosh kw'} \\ + \frac{2}{w} \frac{i}{2\pi} \int_{-\infty}^{+\infty} dk e^{ikx} \tanh kw' \tilde{\Phi}_x(k). \end{aligned} \tag{12}$$

This equation yields the solution in the junction region $\Phi(x)$ neglecting the y dependence. From $\Phi(x)$ we compute $I(x)$ in Eq. (11) and obtain the solution in the passive region by forming $\tilde{\psi}(x,k)$ from Eq. (9) and applying inverse Fourier transform to obtain $\psi(x,y)$. The first term in the rhs of Eq. (12) is due to the external current and in the case of vanishing passive region reduces to $(1/w) \delta(x)$, while for uniform distribution irrespective of w' it gives δ_0/w , where δ_0 is the current density per unit length. The second term is a nonlocal term that arises from the folding of the 2D passive region in the window. One can rewrite the second term as an integral in x so that it can be considered as a mutual inductance term.

Let us remark that Eq. (12) can also be obtained by a variation of the functional F which in the case of zero external current [$\delta(x)=0$] can be written as

$$F = \int_{-\infty}^{+\infty} dx \left(\frac{\Phi_x^2}{2} + 1 - \cos \Phi \right) - \frac{1}{w} \int_{-\infty}^{+\infty} dx \int_{-\infty}^{+\infty} dx' \Phi_x(x) K(x-x') \Phi_x(x'), \quad (13)$$

where $K(x-x')$ is the kernel associated to the right hand side of Eq. (12) and has a Fourier transform

$$\tilde{K}(k) = \frac{\tanh kw'}{k}.$$

Thus the second term of F can be written by using the convolution theorem as

$$\mathcal{I} = \int_{-\infty}^{+\infty} dx \int_{-\infty}^{+\infty} dx' \Phi_x(x) K(x-x') \Phi_x(x') = \frac{1}{2\pi} \int_{-\infty}^{+\infty} dk \tilde{\Phi}_x(-k) \tilde{K} \tilde{\Phi}_x(k). \quad (14)$$

In the limit $w'=0$, Eq. (12) is the 1D static sine-Gordon equation, while for small w' it leads to fluxons with an increased width. To see this we rewrite the second term in the rhs of Eq. (12) by noting that the main contribution to the integral comes from $k \approx 0$, as can be seen by the method of stationary phase. So in the limit of a small w' we use the expansion $(\tanh kw')/k = w' + O(k^2)$ and it yields approximately $(2w'/w) \Phi_{xx}$ by virtue of the inverse Fourier transform. Thus, we obtain for Eq. (12) in this limit (with $\delta=0$) $-\lambda_{\text{eff}}^2 \Phi_{xx} + \sin \Phi = 0$, with $\lambda_{\text{eff}} > \lambda_J (=1)$ given by

$$\lambda_{\text{eff}} = \sqrt{1 + \frac{2w'}{w}}. \quad (15)$$

This can also be obtained by a variational approach of the free energy functional in the special case where the constant phase lines are almost straight lines even in the passive region,⁷ with the variational parameter the width of the kink-like solutions. Expression (15) can be easily understood if we define an effective inductance per unit length in the x direction as the sum of two parallel inductances with $L_J = \mu_0 d/w$ for the window and $L_P = \mu_0 d/2w'$ in the passive region. If we use an effective current density per unit length of wJ_c in the expression for λ_J , we obtain Eq. (15).

In the case of large w' the surface current paths present strong deviations from straight lines and one cannot use the previous result, where we consider the effective inductance of two parallel waveguides. Here one must use a variational approach by assuming explicitly a fluxon type solution inside the window of the form $\Phi_f(x) = 4 \arctan(e^{-x/d})$, where the width d is the variational parameter. Like in Ref. 7 we use the free energy approach and notice that Eq. (12) results from the variation of the functional F . The calculations are easier if one considers $q(x) \equiv (\Phi_f)_x = (2/d) 1/\cosh(x/d)$ with its Fourier transform $\tilde{q}(k) = 2\pi \operatorname{sech}(\pi kd/2)$. Summing all the terms yields the expression for F

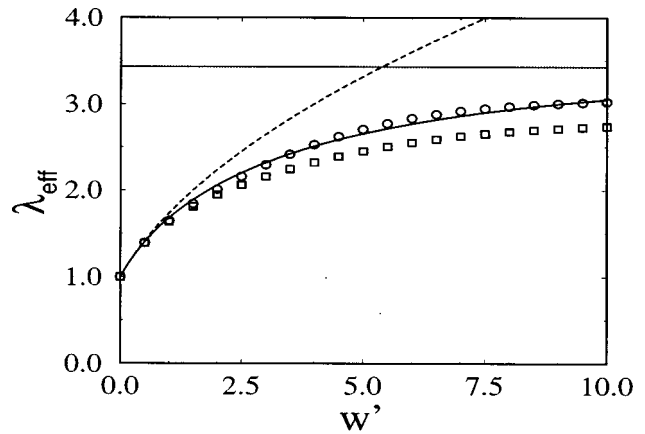


FIG. 2. Plot of the fluxon width $d = \lambda_{\text{eff}}$ vs the passive region extension w' obtained from (a) solution of the variation of $F(d)$ in Eq. (16) (solid line); (b) small w' limit from Eq. (21) (short dashes); (c) infinite passive region from Eq. (23) (long dashes); and (d) numerical solution of nonlocal Eq. (12) for finite lengths with $l = 12$ (circles) and $l = 15$ (crosses).

$$F\{\Phi_f\} = \frac{4}{d} + 4d + \frac{2\pi}{w} \int_{-\infty}^{+\infty} dk \frac{\tanh kw'}{k} \frac{1}{\cosh^2(\pi kd/2)}. \quad (16)$$

For large w' one can approximate the integral in Eq. (16) and recover the logarithmic expression for the magnetic energy in the passive region in the case of radial phase lines, since

$$\int_{1/w'}^{2/\pi d} \frac{dk}{k} = \log \frac{2w'}{\pi d},$$

from which by differentiation of F with respect to d one obtains the effective fluxon width for infinite passive regions⁷

$$d = \frac{\pi}{2w} \left[1 + \sqrt{1 + \left(\frac{\pi}{2w}\right)^{-2}} \right]. \quad (17)$$

The two limits given by Eqs. (15) and (17) obtained respectively for a small and infinite w' should be compared with the value d which minimizes F , i.e., from $dF/dd = 0$. We calculated the solution numerically and plotted the fluxon width in Fig. 2 obtained from the variation of Eq. (16) (solid line) together with the limiting behaviors given by Eq. (15) for $w' \rightarrow 0$ (short dashed curve) and Eq. (17) for $w' \rightarrow \infty$ (long dashed curve). It can be seen that Eq. (15) describes well the situation for $w' \leq 1$, but diverges from the variational result for higher w' . The asymptotic value for $w' \rightarrow \infty$ is given by Eq. (17) to a good approximation giving a $\lambda_{\text{eff}} = 3.43$. This value depends only on the width of the window, which in this case is $w = 1$. The analytical simple formulas and the variational result are derived for an infinite junction by neglecting the tails in the solution. Thus one does not expect them to agree with the numerical solution of the nonlocal sine-Gordon, where the tail for increasing w' is important. In the figure we present the results obtained from the numerical solution of the nonlocal sine-Gordon system in

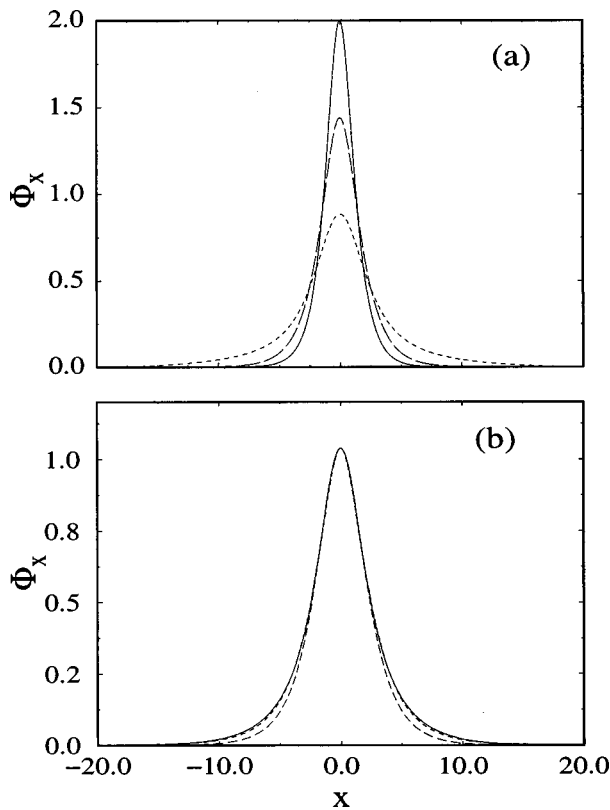


FIG. 3. (a) Plot of $\Phi_x(x)$ for a finite length junction with $l=1$, $w=1$, and $w'=0$ (solid line), 2 (long dashes), 5 (short dashes). (b) The case $w'=2$ (solid line) is fitted by a sech-type form (long-dashed line) and the modified trial function (short-dashed line) including a nonlocal component.

Eq. (12) for $l=12$ (circles) and $l=15$ (squares). We used a cosine transform expansion for the finite length calculation, whose details will be discussed in the next section. The numerical result for the static solution with no external current and magnetic field is fitted by a monoparametric function $Q_s(x) = (2/d)\text{sech}(x/d)$ for the Φ_x , which corresponds to a pure sine-Gordon soliton with an effective width d . This particular fitting is necessary for the sake of comparison since we keep the same form as in the local or nonlocal variational approach. In the numerical simulations for a finite length one expects deviations due to the boundary conditions and therefore a length dependence. It should be remarked that the width of the fluxon is not a sufficient parameter to characterize the solution since the form of the solution is not of a simple sech-type (for Φ_x) but also has a tail component which becomes more important as the size of the passive region increases. In Fig. 3(a) we show the variation of the solution profile for $w'=0,2,5$. We see that as w' increases a solution with essentially two scales becomes apparent. This is evident if we try to fit the case $w'=2$ with a sech-type solution and we see that the agreement is good near the center but is off at the tails. In Fig. 3(b) the fitting (long-dashed line) is done by matching the amplitude of the pulse while its width is automatically determined as in the sine-Gordon soliton. We see that the numerical solution (continuous line) has a slightly smaller width near the center and larger at the tails, stressing again the existence of more than one scale due to nonlocality.

Based on our computer simulations, we remark that the results for large w' with the variational approach may be considerably improved, if we take into account the possibility of nonexponential soliton tails by introducing the following three-parametric trial function

$$\Phi_x = \alpha \frac{2}{d_1} \text{sech}(x/d_1) + 2(1 - \alpha) \frac{d_2}{(x^2 + d_2^2)}.$$

The parameter α is a weighting factor for the two terms which can be considered the solutions for the limiting cases of local ($w' \rightarrow 0$) and completely nonlocal ($w' \rightarrow \infty$) behavior with corresponding widths determined by d_1 and d_2 . The parameter d_2 by fitting the amplitude of Φ_x is given as a function of α and d_1 . Using the earlier trial function we fitted the curve for $w'=2$ [short-dashed line in Fig. 3(b)] and we see that for $\alpha=0.785$ and $d_1=2.055$ (so that $d_2=1.561$) we obtain a much better fitting. From the value of $\alpha=0.785$ we see that the contribution of the algebraic part is significant. For $w'=0.5$, we find $\alpha=0.97$ so that the contribution of the algebraic tail is not so important, but for $w'=5$ we get $\alpha=0.504$ so that it deviates strongly from the local expression and one must solve numerically the integral equation as we do here.

We have therefore shown that the 2D PDE system (1) and (2) describing the static behavior of an infinitely long and thin window junction can be reduced to a 1D integro-differential equation which can be rescaled into the static sine-Gordon equation by changing the spatial unit from 1 ($=\lambda_j$) to λ_{eff} as given by Eqs. (15) or (17). This approximation done in the infinite length case for which no boundary conditions are given in the x direction will be shown to carry on to the finite junction length case in the next section.

III. THE CASE OF A FINITE LONG THIN JUNCTION

We consider now the case of a finite length window junction as shown in Fig. 1(c) together with the mixed inline-overlap boundary conditions. For the general geometry of Fig. 1(a), it is difficult to treat the problem of a general passive region because of the complexity of the Green's function. We will therefore make the following simplifying assumptions: (i) the junction is infinitely thin, (ii) we will neglect the longitudinal passive regions so that the design reduces to the one in Fig. 1(c). The latter hypothesis can be justified by the numerical experiments for the static properties⁷ which showed that only the lateral part of the passive region contributes to λ_{eff} in accordance with the observations of Ref. 5. In any case the design of Fig. 1(c) can be also achieved experimentally. In the following we will assume for simplicity in the calculations that the current densities α , δ , and magnetic field H are uniform.

In this case we solve the 2D PDE system (1) and (2) in the window domain $|x| \leq \frac{l}{2}$, $|y| \leq w/2$ and the passive region domain $|x| \leq \frac{l}{2}$, $w/2 \leq |y| \leq w/2 + w'$, together with the interface and lateral boundary conditions [see Eq. (5)] supplemented by the end boundary conditions

$$\phi_x|_{x=\pm \frac{l}{2}} = H \pm \frac{\alpha}{2}, \quad \psi_x|_{x=\pm \frac{l}{2}} = \left(H \pm \frac{\alpha}{2} \right). \quad (18)$$

We can follow the same procedure as in the infinite length case and obtain Eq. (7) but the Laplace problem in the passive region involves now boundary conditions in x . To reduce these to homogeneous Neumann boundary conditions, we introduce the auxiliary function $f(x)$ and the new variable $\theta(x,y)$ such that

$$\theta(x,y) = \psi(x,y) - f(x) \quad \text{with}$$

$$f(x) \equiv \left\{ Hx + \frac{\alpha}{4l} \left[\left(x - \frac{l}{2} \right)^2 + \left(x + \frac{l}{2} \right)^2 \right] \right\} \quad (19)$$

so that the problem for θ is now

$$\Delta \theta = -\frac{\alpha}{l}, \quad (20)$$

$$\theta_x|_{x=\pm \frac{l}{2}} = 0, \quad \theta_y|_{y=w/2} = \frac{w}{2}I, \quad \theta_y|_{y=w/2+w'} = \frac{\delta}{2}, \quad (21)$$

which can be solved by expanding θ in cosine Fourier series in x

$$\theta(x,y) = \sum_n \theta_n(y) \cos k_n(x + l/2)$$

where $k_n = \pi n/l$ and

$$\theta_n(y) = \frac{1}{l} \int_{-l/2}^{l/2} \theta(x,y) \cos k_n \left(x + \frac{l}{2} \right) dx,$$

from which we obtain the solution just like in the infinite junction case except for the last term

$$\theta_n(y) = A_n \cosh k_n \left(y - \frac{w}{2} \right) + B_n \sinh k_n \left(y - \frac{w}{2} \right) + \frac{\alpha_n}{lk_n^2},$$

where A_n and B_n are given by Eq. (9) if $k \rightarrow k_n$, $\tilde{\delta} \rightarrow \delta_n$, $\tilde{I} \rightarrow I_n$. Notice here that $\alpha_n = \alpha \delta_{n0}$ and $\delta_n = \delta \delta_{n0}$, where δ_{n0} is the Kronecker symbol. One can proceed as in the infinite length case and calculate

$$\theta_n \left(\frac{w}{2} \right) = A_n + \frac{\alpha_n}{lk_n^2}, \quad (22)$$

connect it with Eq. (7) for small junction width w and identify $\psi(x, w/2)$ with $\Phi(x)$. From Eqs. (20)–(22) we can extract I_n

$$I_n(x) = \frac{\delta_n}{w \cosh kw'} - \frac{1}{w} \left(2k_n \theta_n + \frac{2\alpha_n}{lk_n} \right) \tanh k_n w'. \quad (23)$$

To make the connection with Φ we need to express θ_n as a function of ψ_n . For that we calculate the coefficients of the cosine Fourier transform for each side of Eq. (19) and obtain $\theta_n = \psi_n - f_n$, where f_n is the cosine Fourier component of $f(x)$ and using $\Phi_n = f_n + \theta_n(w/2)$ we have

$$\begin{aligned} I &= \sum_n I_n \cos k_n \left(x + \frac{l}{2} \right) \\ &= \frac{\delta}{w} - \frac{2}{w} \sum_n \left(\Phi_n - f_n - \frac{\alpha_n}{lk_n^2} \right) k_n \tanh k_n w' \\ &\quad \times \cos k_n \left(x + \frac{l}{2} \right). \end{aligned} \quad (24)$$

Replacing for I in Eq. (7) yields the final integro-differential equation describing the thin window junction

$$\begin{aligned} -\Phi_{xx} + \sin \Phi &= \frac{\delta}{w} - \frac{2}{w} \sum_n \left(\Phi_n - f_n - \frac{1}{lk_n^2} \alpha_n \right) k_n \\ &\quad \times \tanh k_n w' \cos \left[k_n \left(x + \frac{l}{2} \right) \right]. \end{aligned} \quad (25)$$

On the right hand side the first term is the usual overlap current while the second represents the contribution from the bulk of the passive regions exactly like the second integral on the right hand side of Eq. (12). The last two terms are associated with the boundary conditions in the x direction on the passive region. We will now proceed to estimate these terms and show that Eq. (25) can be reduced in the same way as Eq. (12) can be reduced to an effective sine-Gordon model with appropriate rescalings by λ_{eff} .

The second term on the rhs of Eq. (25) yields the rescaling of Φ_{xx} using the same approximation as for the infinite case when the idle region extension w' is small and the third term arose from the boundary conditions (through the auxiliary function f_n) and we can ignore. Then the problem of a “truncated” window junction as shown in Fig. 1(c) can be approximated when the passive region is not very large by the effective sine-Gordon model with the corresponding boundary condition

$$-\Phi_{xx} \lambda_{\text{eff}}^2 + \sin \Phi = \frac{\delta}{w}, \quad \text{with } \Phi_x|_{x=\pm l/2} = H \pm \frac{\alpha}{2}, \quad (26)$$

where λ_{eff} is given by Eq. (15) and includes the effect of nonlocality.

Notice that the total current I satisfies

$$I = \int_{-l/2}^{l/2} \sin(\Phi) dx = \frac{\delta l}{w} + \left(1 + 2 \frac{w'}{w} \right) \alpha,$$

which is exactly the value obtained for the 2D PDE (1). Introducing the reduced length $l' = l/\lambda_{\text{eff}}$ and current density $\alpha' = \alpha/\lambda_{\text{eff}}$ we obtain $I = \lambda_{\text{eff}}(\delta l'/w + \alpha')$. We also normalize the x variable and magnetic field H by introducing $x' = x/\lambda_{\text{eff}}$ and $H' = H\lambda_{\text{eff}}$ so that Eq. (26) with the boundary conditions become

$$-\Phi_{x'x'} + \sin \Phi = \frac{\delta}{w} \quad \text{with } \Phi_{x'}|_{x'=\pm l'/2} = H' \pm \frac{\alpha'}{2}. \quad (27)$$

It is therefore very simple to obtain the $I_{\text{max}}(H)$ curve for Eq. (26) by computing $I'_{\text{max}}(H')$ for Eq. (27) and rescale the current I' by λ_{eff} and the magnetic field H' by $1/\lambda_{\text{eff}}$.

This result could be inferred from physical considerations. From the above we expect that since the length λ_{eff}

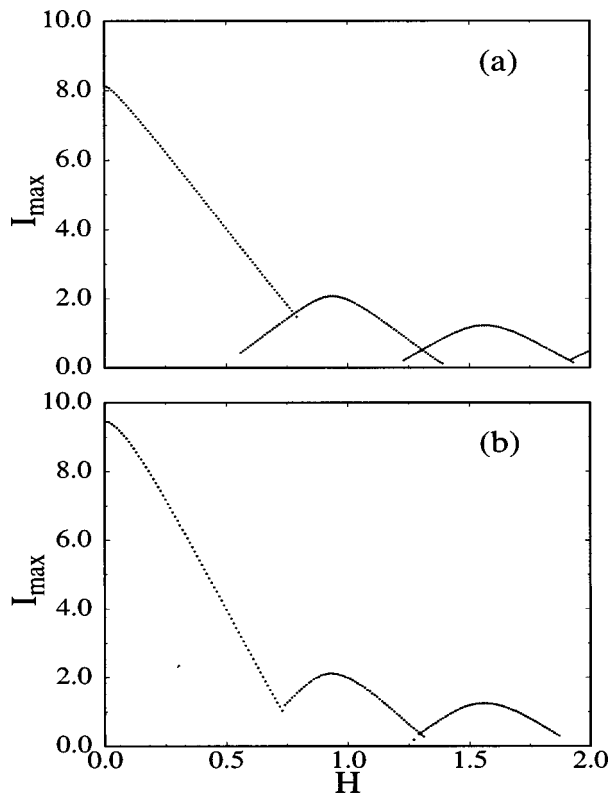


FIG. 4. Plot of $I_{\max}(H)$ curve for the finite domain nonlocal junction with inline current feed. The parameters are $l=10$, $w=1$, (a) $w'=2$, (b) 5.

increases with the extend of the passive region, the maximum current at zero magnetic field, $I_{\max}(0)$ also increases proportionally to λ_{eff} if we are not near saturation. On the other hand, since the maximum current vanishes when a full fluxon enters the junction, we expect that the critical magnetic field H_c will decrease inversely proportional to λ_{eff} . This is what the numerical simulations in the next section will show (see Fig. 4). Some insight in that direction can be gained if we choose a normalized length and introduce $\bar{x} = x/\lambda_{\text{eff}}$ so that the new junction length is $\bar{l} = l/\lambda_{\text{eff}}$. Then we see from Eq. (25) that H becomes $H\lambda_{\text{eff}}$ and α becomes $\alpha/\lambda_{\text{eff}}$. This means that we can solve the 1D static sine-Gordon in the reduced length and then multiply the current by λ_{eff} and divide the magnetic field by λ_{eff} . The difference in scaling of the magnetic field and the current essentially arises from their respective contributions to the symmetry of the boundary condition in Eq. (26).

There are therefore two levels in the approximation which reduces the uniform window junction and the 2D PDE system (1) to the effective 1D sine-Gordon Eq. (26). First is the reduction of the uniform window to a lateral passive region by eliminating the longitudinal passive regions. After that comes the reduction of the integro-differential sine-Gordon Eq. (12) to the effective model of Eq. (26). In the following section, we will show that the latter model provides a good approximation to the $I_{\max}(H)$ curves obtained for the 2D model and that the main limitation in the case of small width junctions comes from eliminating the longitudinal passive regions. Thus one could solve the scaled sine-

Gordon equation with the usual boundary conditions in x for the magnetic field $\Phi_x = h$ and then rescale the plot $\delta(h)$ into $\lambda_{\text{eff}}\delta(h/\lambda_{\text{eff}})$ to obtain the behavior for the real junction.

IV. NUMERICAL RESULTS FOR 2D WINDOW JUNCTIONS

For the numerical evaluation of the single static fluxon in a finite length junction with no bias current $\delta=0$, $\alpha=0$, and $H=0$, we can use the discrete cosine series with the auxiliary function $f(x)=0$, which automatically satisfy the homogeneous boundary conditions $\Phi_x(x=\pm l/2)=0$. The problem reduces to the solution of $K(k)\tilde{\Phi}_k = -[\sin\tilde{\Phi}]_k$ where $k \equiv k_n = \pi n/l$, the subscript “ k ” denoting the k_n cosine component and

$$K(k) = k^2 + \frac{2k}{w} \tanh(kw'). \tag{28}$$

Thus, we end up with a system of nonlinear algebraic equations for the cosine Fourier components of $\Phi(x)$. This can be easily solved by a simple relaxation iteration scheme where we added in both sides of the equations the term $r\tilde{\Phi}_k$ (with $r=1.5$) to speed up the convergence and get the solution with very high precision within a few iterations. We stop the calculation when the norm of the difference of two subsequent iterants is less than 10^{-6} . We calculate the single fluxon width as a function of w' , while the junction length l is kept constant (see Fig. 2).

In the numerical calculation of the I_{\max} vs H , for the nonlocal 1D model given for the finite length in Sec. III, the inline boundary conditions due to the imposed current and magnetic field, are $\Phi_x(x=\pm l/2) = H \pm \alpha/2$. We use $\Phi(x) = \Theta(x) + f(x)$ and the iterative equation for $\tilde{\Theta}_k$ is obtained if we put $\tilde{\Phi}_k^{(n)} \rightarrow \tilde{\Theta}_k^{(n)}$ except in the $\sin\Phi^{(n)} \rightarrow \sin[\Theta^{(n)} + f(x)]$ in the previous paragraph. For homogeneous current feed, only the $k=0$ component of $[f(x)]_k$ is different from zero. This enters the equation for $\tilde{\Theta}_k$ in a nonlinear function so that it will influence all the components. However, in general only a few components will be sufficient to get a well convergent solution, since the $\tilde{\Theta}_k$ decay exponentially fast. We performed the calculations for $w'=0,2,5$ with inline current feed ($\delta=0$). The case with $w'=0$ (sine-Gordon limit)¹⁴ served as a test for the accuracy of our numerical code. We find that for $H=0$ the numerically calculated value differs from the correct theoretical value $I_{\max}(0)=4$, only by about 0.1%. As in the 2D calculations, the zero-field critical current increases considerably even for moderate w' values, reaching 95% of its saturation value already for $w'=5$ (see Fig. 4). On the other hand, the value H_c where the critical current becomes zero for the first time decreases by a factor which is about 2 or larger for $w' \geq 2$.

We have also solved the coupled PDE system (1) and (2) in the case $L_{p,j} \equiv 1$. Then Eq. (1) is completely equivalent to the equation describing the junction and passive regions $\Delta\phi = I_j(x,y)\sin\phi$, where $I_j(x,y)=0$ (1) in the passive (window) area, respectively, together with the boundary conditions on the passive region interface. Then one can linearize using the Newton iterative method, which is known to

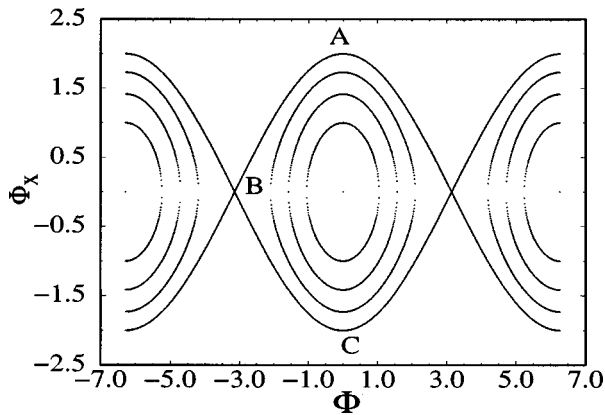


FIG. 5. Phase portrait (Φ_x, Φ) for the equation $\Phi_{xx} = \sin \Phi$.

converge quadratically. The practical implementations of the procedure has been done using the ELLPACK software¹² and the details of this implementation can be found in Ref. 13. At $I = I_{\max}$ instability sets in and double precision is necessary. At that point the linear operator in the Newton linearized scheme becomes singular. This is completely equivalent to the dynamical instability of the static solution in the time-dependent sine-Gordon system, so that the threshold obtained is of physical interest. Then stepping in current and magnetic field one can obtain the different $I_{\max}(H)$ branches corresponding to 0-1 fluxon, 1-2, ..., etc. The effective local model of Eq. (26) was solved following the same procedures and we chose the same junction of parameters $l = 10$, $w = 1$ which we have embedded in passive regions of different uniform extensions w' along the window perimeter.

We have first considered the case of an inline current feed, i.e., for $\delta = 0$. For a long junction the $I_{\max}(H)$ curve for the 0-1 fluxon branch is linear and for $H = 0$ one has $I_{\max} = 4$ (Ref. 14) corresponding to the penetration of the magnetic field in a region of extension 2 (λ_j) at each end of the junction. These features can be seen on the phase space (Φ, Φ_x) of the pendulum Eq. (26) shown in Fig. 5. The solution for $H = 0$ is such that $\phi = \pi$ at each end and corresponds in the case of a long junction to the orbit close to the separatrix $\Phi_x^2/2 = \pm(1 - \cos \Phi)$, along AB for the right end and BC for the left end. When the magnetic field is increased the left hand phase decreases gradually (C moves towards B) while the right (at A) remains at π so that the linear decrease of the current α is given by $\Phi_x|_{x=l/2} = 2 = H + \alpha/2$. The value H_c gives a zero current and corresponds to a one fluxon solution.

When the passive region extension w' is small the window junction exhibits the same qualitative features as can be seen from Fig. 6(a) for $I_{\max}(H)$ at $w' = 0.5$ [all around as in Fig. 1(b)]. Notice however that $I_{\max}(0)$ is significantly greater than 4 and that the magnetic field giving a zero current H_c is reduced from 2 to around 1.4. For this geometry $\lambda_{\text{eff}} = \sqrt{2} \approx 1.41$ and the plot obtained from the solution of Eq. (26) (shown as a dashed line) is in excellent agreement with the results of the 2D simulation. This means that at least for small w' not only an effective local 1D problem can be constructed but the passive region at the ends is not so important, since the 1D sine-Gordon is solved only in the

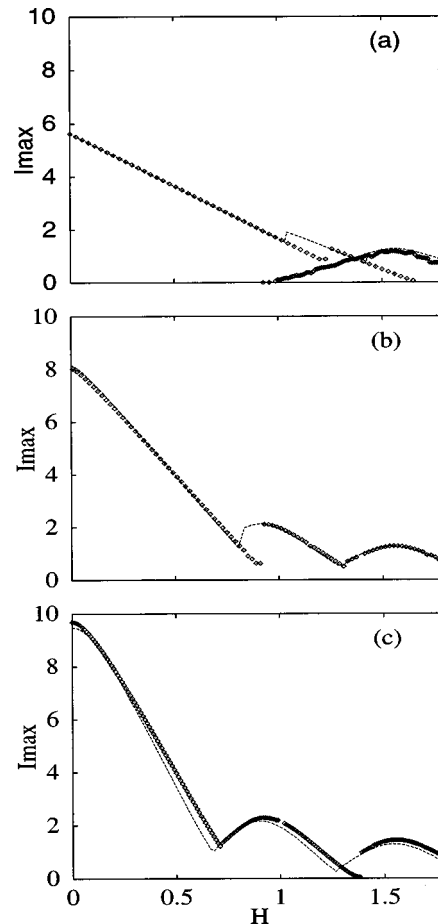


FIG. 6. Three first branches of the $I_{\max}(H)$ curve for a window junction ($l = 10$, $w = 1$) with inline current feed, for the uniform window around (points) and the effective model (dashed lines). (a) $w' = 0.5$, (b) $w' = 2$, and (c) $w' = 5$.

length of the window. As the passive region extension w' is increased to 2 [Fig. 6(b)] and 5 [Fig. 6(c)] $I_{\max}(0)$ increases and saturates at 10 as expected while H_c decreases. The first branch loses its linearity and the behavior tends toward the Fraunhofer pattern $(\sin Hl)/H$ typical of short junctions where the different branches do not overlap. For $w' = 2$ and 5, the values of λ_{eff} obtained from variation of Eq. (15) 2.23 and 3.31 yield a quite good agreement of the plot $\lambda_{\text{eff}}\alpha$ vs H/λ_{eff} obtained from the solution of Eq. (26) with the one given by the direct two-dimensional solution of Eqs. (1) and (2).

Therefore the loss of linearity of the first branch, the increase of $I_{\max}(0)$ and the decrease of H_{c1} indicate that the behavior of a long junction in a passive region is the one of a shorter junction of length l/λ_{eff} . A junction of length 10 becomes a "small junction" if the passive region extension w' is big enough approaching the diffraction-like pattern for $I_{\max}(H)$. A qualitatively similar picture is seen in the experiments although the boundary conditions on the current are not of inline type and the ratio of inductances in the active and passive regions is different from 1.

The other type of current feed, the so-called overlap design is such that $\alpha = 0$. In the case of a long junction, current will accumulate at each end of the window giving it also an inline character. This will result in a maximum current at

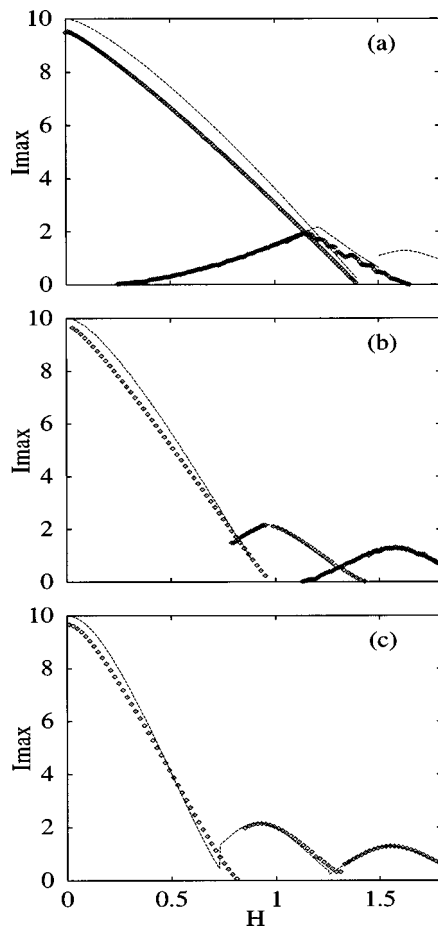


FIG. 7. Same as Fig. 6 for overlap current feed.

zero magnetic field slightly smaller than the area $l \times w$. We therefore expect that the approximation of neglecting the longitudinal parts of the passive region leading to Fig. 3 becomes less good than in the inline case. This will of course result in a less adequate correspondence between the effective model and the 2D solution. Figure 7(a) shows the $I_{\max}(H)$ curves for both the 2D solution and the effective model using overlap current feed for a passive region width $w' = 0.5$. The slight deficit in $I_{\max}(0)$ with respect to 10 can be noticed together with the fact that the effective model overestimates by 10% the total current. This overestimation naturally occurs because of the effect mentioned earlier. For smaller currents and larger magnetic fields from which the y dependence of the solution is less important, the agreement is very good. Notice also that the value $H_c = 1.4$ is in full agreement with the one for inline feed seen in Fig. 6(a) as expected because of the correspondence of the boundary conditions when $\alpha = \delta = 0$. When w' is increased to 2 and 5 as shown in Figs. 7(b) and 7(c), the deficit of $I_{\max}(0)$ is improved but still as expected the effective model does not yield a very good agreement for large values of the current. For large enough w' , it seems that the lateral side of the window attracts most of the current, approaching thus the overlap-like boundary conditions.

V. DISCUSSION AND CONCLUDING REMARKS

In this article we showed that the important length is λ_{eff} , which must be determined self consistently, i.e., by the

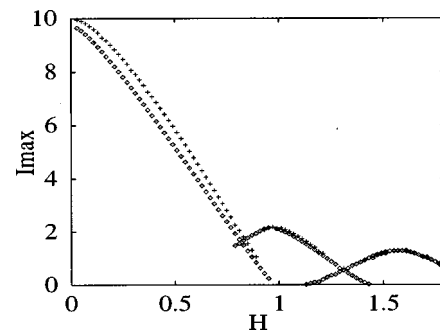


FIG. 8. Comparison of the $I_{\max}(H)$ curve for the uniform window junction (squares) of Fig. 7(b) with the one obtained for a junction where the longitudinal passive regions have been removed (crosses).

solution of the integro-differential equation for the phase distribution of a single fluxon. This is the important length over which all variations must be considered. Once λ_{eff} is known all static properties can be approximated by solving a reduced 1D problem over the length l/λ_{eff} and then rescaling the current and the magnetic field as discussed earlier. We chose nevertheless as the unit of length the Josephson penetration length ($\lambda_J = 1$) in the pure junction for two reasons. It is the important parameter when $w' = 0$ and also λ_{eff} must be calculated self consistently, and is not known beforehand. For some geometries one can estimate it. Of course, the earlier facts must be taken very seriously in experimental work when determining the characteristic length scale from the I_{\max} vs H curve or the maximum critical current density. A way to bypass the self-consistent solution, or better the solution of an integro-differential equation is the effective model we have constructed, which works over a range of geometric parameters with the limitations stated later. Thus the self consistency is reduced to the solution of a simple sine-Gordon 1D equation with the rescalings on the length the magnetic field and the current discussed earlier. Outside the range of validity of the effective model one can solve the nonlocal 1D problem.

A limitation of the effective model approach is due to the lack of correspondence between the 2D geometry of the phase lines in the case of a window uniformly surrounded by a passive region and a window with only lateral passive regions. In fact, the comparison of the maximum current $I_{\max}(H)$ for the two geometries shows that the latter always gives an overestimate of the maximum current as shown in Fig. 8 which compares the $I_{\max}(H)$ for the uniform window junction of Fig. 7(b) with the one for the junction with only lateral passive regions. To understand this effect we have plotted the phase lines using the same contour levels for the two geometries for $H = 0.11$ and $I = 9.1$ in Fig. 9. One can then remark that the dip appearing in the left hand side of the junction for the uniform geometry indicates an accumulation of current which is absent for the device for which the longitudinal passive region has been removed. Notice however the good agreement of the overall set of contour lines explaining the 10% difference which is seen in this case between the maximum current values. This is especially true near the phase line $\phi = \pi/2$ (heavy contour line) that gives the most important contribution to the tunneling current.

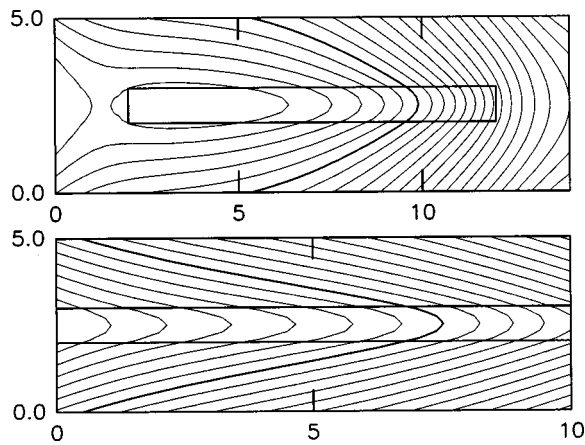


FIG. 9. Contour lines of the phase for the two geometries of Fig. 8, for $H = 0.21$ and the corresponding $I_{\max} = 8.20$ for the sample with a longitudinal passive region shown on the top plate and a current $I_{\max} = 8.84$ for the sample without a longitudinal passive region shown on the bottom plate. The level curves are the same for both plots with a level spacing of 0.13. The contour line corresponding to $\pi/2$ has been highlighted and the minimum is on the left of the pictures.

Near this contour the two patterns are quite similar (remark the different length scales in the two patterns). The difference is small for higher fields where the patterns become 1D-like. The accumulation of phase gradients at the ends of the junction leads to the slight inline character of the current feed reaching the junction. We have tried to model phenomenologically this effect by assuming a uniform density along the perimeter of the window and assume α and δ to be non-zero in the effective model calculation, however, this did not yield a good correspondence with the 2D calculations. The percentage of inline versus overlap current feed should then be adjusted depending on w' .

A more serious limitation of the approach resides in the cases when w is large so that the two-dimensional structure of the phase distribution cannot be neglected. Figure 10(a) shows $I_{\max}(H)$ for a junction of length $l = 10$, width $w = 6$ in a uniform passive region of extension $w' = 2$ for an overlap current feed and in Fig. 10(b) for an inline current feed. The inline case is well approximated by the simple model. In the overlap case the maximum current does not reach the value given by the area but a much smaller value given by the penetration depth of the magnetic field inside the junction. The result can only be obtained by a 2D numerical calculation. The absence of longitudinal passive region would give an actual overlap situation [in particular at $H = 0$ with $I_{\max}(0) = 40\lambda_{\text{eff}}$], which from the simple expression is about $\lambda_{\text{eff}} = 1.25$. Thus it turns out that in this case a significant contribution comes from an inline component at the perimeter, so that in the corner the inline and overlap components feel the saturation due to the maximum critical tunneling current sooner. In fact, the outside bias distribution is not so crucial for a large idle region. Thus in this case the effective model approach gives a strong overestimation $I_{\max}(0) = l \times w$. This situation is analogous to the case of a pure junction of wide area¹⁵ for which the averaging approach of Eq. (6) does not yield an accurate representation of the solution inside the junction. Figure 11 shows the contour lines for the

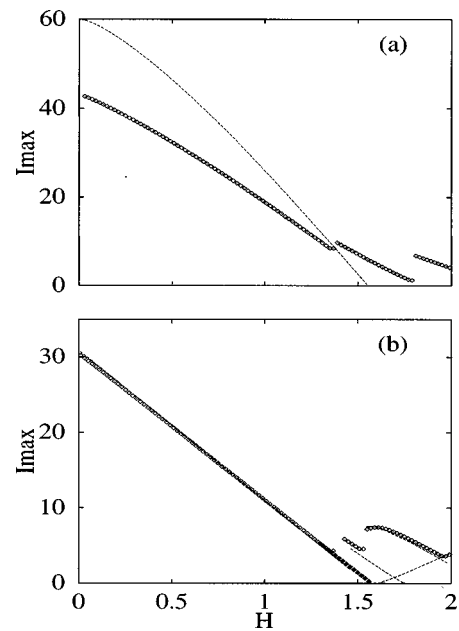


FIG. 10. Three first branches of the $I_{\max}(H)$ curve for a wide window junction with $l = 10$, $w = 6$, and $w' = 2$. (a) Overlap and (b) inline boundary conditions. The dashed line is from the 1D model.

phase for this wide window junction, and one clearly sees the boundary layers of size $2\lambda_{\text{eff}} \approx 2.4$ on each lateral side of the junction. In this case a more precise modeling of the junction would involve a Fourier expansion in the y direction. The case of inline geometry is much more simple because then the 2D character of the solution can still be neglected and the validity of the model depends on the validity of the approximation of neglecting the longitudinal parts of the passive region which is good for this type of current feed.

In this study we have not addressed the case of an inhomogeneous current distribution. This is mainly for technical reasons, there are no difficulties in principle. In this case all harmonics of α and δ should be kept. Then the overlap cur-

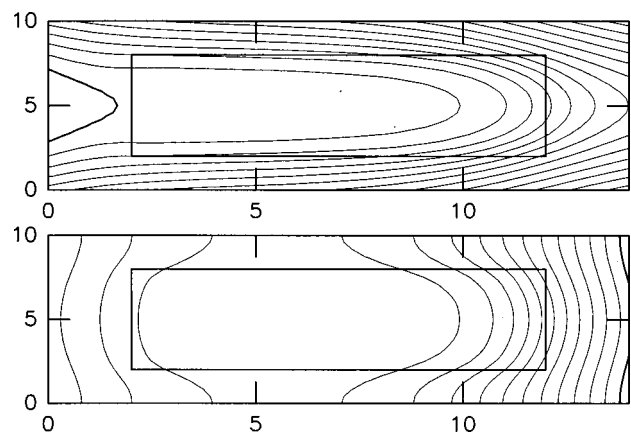


FIG. 11. Contour lines of the phase for a magnetic field $H = 0.51$ and the corresponding $I_{\max} = 30.71$ for the overlap current feed shown on top and $I_{\max} = 20.61$ for the inline current feed shown on the bottom. For the top plate, the phase range is $5.75 < \phi < 13.40$ while for the bottom plate it is $0 < \phi < 6.62$, the minima are on the left of the pictures. The level curves are the same for both plots with a level spacing of $\pi/6$ and the contour line corresponding to 2π has been highlighted.

rent terms in the effective model are not so simple as in Eq. (26). In any case a fork type structure up to the junction can assure a uniform bias distribution.¹⁶

An important physical effect which we have not considered in this study is the difference in the surface inductances between the active and passive regions. In this case the reduction of the uniformly surrounded junction of Fig. 1(b) to the lateral passive region junction of Fig. 1(c) is not physically meaningful, for the boundary conditions assumed, because this introduces discontinuities of the x derivative of the phase at the interface. In this case (lateral window) the solution has some delta function singularities at each corner of the interface, and this problem cannot be used to understand the uniform window case. This will require different boundary conditions than the ones adopted here. In this article we considered only the static properties and did not take into account the effect of damping, which, however can influence the transient behavior. Damping due to quasiparticle tunneling or surface losses will play an important role in the current voltage characteristics, i.e., the dynamic behavior of the junction.

ACKNOWLEDGMENTS

Part of this work was supported by an INTAS Grant (No. 94-1783) and two PENED Grant (Nos. 2028/1995, 602/1995). V.K. and J.G.C. acknowledge the hospitality of the University of Crete. The visit of J.G.C. was made possible by a grant under the Greek-French collaboration agreement and the visit of V.K. by a grant from the University of Crete.

- ¹A. Barone and G. Paterno, *Physics and Applications of the Josephson Effect* (Wiley, New York, 1982).
- ²K. Likharev, *Dynamics of Josephson Junctions and Circuits* (Gordon and Breach, New York, 1986).
- ³See papers in *Proceedings of Nonlinear Superconducting Devices and High- T_c Materials*, edited by R. D. Parmentier and N. F. Pedersen (World Scientific, Singapore, 1995).
- ⁴N. Thyssen, A. V. Ustinov, H. Kohlstedt, J. G. Caputo, S. Pagano, and N. Flytzanis, *Proceedings of Nonlinear Superconducting Devices and High- T_c Materials* (World Scientific, Singapore, 1995), p. 107.
- ⁵R. Monaco, G. Costabile, and N. Martucciello, *Proceedings of Nonlinear Superconducting Devices and High T_c Materials* (World Scientific, Singapore, 1995), p. 115.
- ⁶C. Lee, *IEEE Trans. Appl. Supercond.* **1**, 121 (1991); C. Lee and A. Barfknecht, *ibid.* **2**, 67 (1992).
- ⁷J. G. Caputo, N. Flytzanis, and E. Vavalis, *Int. J. Mod. Phys. C* **7**, 191 (1996).
- ⁸*Computer Techniques for Electromagnetics*, International Series of Monographs in Electrical Engineering, Vol. 7, edited by R. Mittra (Pergamon, New York, 1973).
- ⁹L. D. Landau and E. M. Lifchitz, *Theoretical Physics* (Pergamon, New York, 1986), Vol. 6.
- ¹⁰S. Maggi and V. Lacquaniti, *J. Low Temp. Phys.* **106**, 393 (1997).
- ¹¹J. C. Eilbeck, P. S. Lomdahl, O. H. Olsen, and M. R. Samuelsen, *J. Appl. Phys.* **57**, 861 (1985).
- ¹²J. R. Rice and R. F. Boisvert, *Solving Elliptic Problems Using ELLPACK* (Springer, New York, 1985).
- ¹³J. G. Caputo, N. Flytzanis, and E. Vavalis, *Int. J. Mod. Phys. C* **6**, 241 (1995).
- ¹⁴C. S. Owen and D. J. Scalapino, *Phys. Rev.* **164**, 538 (1967).
- ¹⁵J. G. Caputo, N. Flytzanis, Y. Gaididei, and E. Vavalis, *Phys. Rev. E* **54**, 2092 (1996).
- ¹⁶A. Matsuda, *Phys. Rev. B* **34**, 3127 (1985).